B.Sc. in Electrical and Electronic Engineering Thesis

SPR Bio-sensor based on Photonic Crystal Fiber

Submitted by

Tanvir Alam Roni
1506169

Rifat Hassan
1506177

Supervised by

Dr. Mohammad Faisal

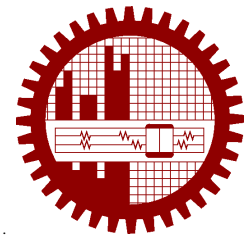

Department of Electrical and Electronic Engineering
Bangladesh University of Engineering and Technology

Dhaka, Bangladesh

February 2021

CANDIDATES' DECLARATION

This is to certify that the work presented in this thesis, titled, "SPR Bio-sensor based on Photonic Crystal Fiber", is the outcome of the investigation and research carried out by us under the supervision of Dr. Mohammad Faisal.

It is also declared that neither this thesis nor any part thereof has been submitted anywhere else for the award of any degree, diploma or other qualifications.

Tanvir Alam Roni
1506169

Rifat Hassan
1506177

CERTIFICATION

This thesis titled, **"SPR Bio-sensor based on Photonic Crystal Fiber"**, submitted by the group as mentioned below has been accepted as satisfactory in partial fulfillment of the requirements for the degree B.Sc. in Electrical and Electronic Engineering in February 2021.

Group Members:

Tanvir Alam Roni

Rifat Hassan

Supervisor:

Dr. Mohammad Faisal
Professor
Department of Electrical and Electronic Engineering
Bangladesh University of Engineering and Technology

ACKNOWLEDGEMENT

Authors wish to express their deepest gratefulness to God Almighty, Allah for the successful completion of this thesis work. Special thanks to our supervisor Professor Mohammad Faisal, PhD for his encouragement and valuable suggestions throughout the thesis work. It has been an honor and great pleasure for us to work under his supervision. We wish to thank our families for their constant supports throughout our undergraduate life. The author would like to extend their deep sense of gratitude to Md. Saiful Islam, PhD, Shah Md. Salimullah, Md. Al Imran Abir for their valuable suggestions and co-operation.

Dhaka
February 2021

Tanvir Alam Roni

Rifat Hassan

Contents

CANDIDATES' DECLARATION i

CERTIFICATION ii

ACKNOWLEDGEMENT iii

List of Figures vi

List of Tables vii

ABSTRACT viii

1 Introduction 1

1.1 Background . . . 1
1.2 Photonic Crystal Fiber . . . 2
1.3 Surface Plasmon Resonance . . . 3
1.4 Surface Plasmon Polariton . . . 4
1.5 Optical Sensors . . . 5
1.6 Finite Element Method . . . 5
1.7 Our Goal . . . 6

2 Brief Discussion: Optical Sensor 7

2.1 Working Principles . . . 7
2.2 Cross-section . . . 7
2.3 Performance Matrices . . . 10

3 Our Design 12

3.1 Objective . . . 12
3.2 Design 1: Dual Side Polished . . . 13
3.2.1 Numerical Analysis . . . 13
3.2.2 Parameters Optimization . . . 17
3.3 Design 2: Circular . . . 18
3.3.1 Numerical Analysis . . . 20
3.4 Comparison With Previously Reported Sensors . . . 21

4 Conclusion **22**

References **23**

A MATLAB Codes **26**

A.1 Code Snippet For Plotting Amplitude Sensitivity 26

A.2 Code Snippet For Plotting Confinement Loss 27

List of Figures

1.1 Structure of photonic crystal fiber: a) index-guiding PCF, b) photonic bandgap PCF. 2
1.2 Surface plasmon resonance (SPR). 3
1.3 Surface plasmon polariton. 5

3.1 Cross section of Design 1. 12
3.2 Electrical field distribution in a core and b spp mode. 13
3.3 Phase-matching of core and SPP mode for optimized parameters. 14
3.4 Confinement loss for a na = 1.21-1.25, b na = 1.26-1.3, c na = 1.31-1.35 and d na = 1.36-1.34. 15
3.5 Amplitude sensitivity for a na = 1.21-1.25, b na = 1.26-1.3, c na = 1.31-1.35 and d na = 1.36-1.39. 16
3.6 Effect of a air hole diameter (d_1) and b pitch distance (Λ). 17
3.7 Effect of a gold layer thickness (t_g) and b analyte thickness (t_a). 18
3.8 Cross section of Design 2. 18
3.9 Confinement loss fora) na = 1.21-1.25, b na = 1.26-1.3, c na = 1.31-1.35, d na = 1.36-1.38 and e na = 1.39-1.4. 19
3.10 Amplitude sensitivity for a na = 1.21-1.24, b na = 1.26-1.29, c na = 1.31-1.34, d and e na =1.39. 20

List of Tables

ABSTRACT

The main goal of this thesis is to study the characteristics of the SPR biosensor based on photonic crystal fiber and design a novel sensor having an improved sensing performance. We design a dual side polished photonic crystal fiber (PCF) based biosensor with numerical analysis using the finite element method (FEM) for sensing applications. We use gold (Au) as plasmonic material. Our simulation results show an improved dynamic sensing range, ranges from 1.21 to 1.40, operated in the optical to near-infrared (IR) region (0.42-1.0) μm. Moreover, the sensor obtains maximum amplitude and wavelength sensitivity of 1277.47 RIU^{-1} and 5000 nm/RIU respectively with a sensor resolution of 2×10^{-5}.

Chapter 1

Introduction

1.1 Background

Surface Plasmon Resonance (SPR) is an optical phenomenon which can be defined as the collective oscillation of free electrons on the interface between the dielectric and metal. When the wavelength of the surface electrons matches with that of the incoming photons, resonance occurs. At the resonant wavelength, maximum loss for a given analyte is obtained. Any tiny-tiny little changes in the RI causes the peak shift and unknown analyte can be detected by observing the shift of loss peak and corresponding wavelength [1, 2].

SPR sensors are now being widely used for different sensing applications such as medical diagnostic, medical testing, bio-chemical and bio-organic sample detection [3]. The current SPR sensors have been designed based on the Kretschmann and Reathers exploiting attenuated total reflection (ATR) mechanism and also known as prism based SPR sensors [4]. But, they require many supporting (optical and mechanical) components. As a result these sensors are bulky, costly and incompatible for remote sensing [1, 5, 6]. To solve these limitations, conventional optical fiber based miniaturized sensors have been introduced. They have successfully overcome the limitations. They have features like simple and flexible sensor design, remote sensing, continuous analysis and in situ monitoring. They also have lower confinement loss than before. Moreover, conventional optical fibers prevent electromagnetic interference, mechanically stable and cause low confinement loss in the visible range. But they offer less freedom for tuning the design parameters [7].Recently, SPR sensors based on PCFs are getting higher acceptance than the conventional fiber because of their controllable light-guiding mechanism, strong birefringent properties as well as highly flexible structural design [8, 9].

Photonic Crystal Fiber (PCF) is compact and lightweight, which permits miniaturization of the sensors, making them attractive for remote sensing applications [7, 10]. The plasmonic metal layer can be coated outside the fiber surface or inside of the air holes. Incident light is launched

at one end and the response is observed from the other end. And, For achieving strong coupling between the core mode and SPP mode, we can optimize the design of PCF that consequently improves sensing performance [8, 11].

Different well-known plasmonic materials such as gold, silver, copper, graphene, and titanium nitride are used to excite SPR. However, gold (Au) and silver (Ag) are the most commonly used as plasmonic material. Gold is chemically stable, bio-compatible, and also gives rise to a larger wavelength shift. Whereas, silver gives a sharper resonance peak then gold. The silver becomes oxidized in a humid environment and this reduces the analyte detection accuracy [11]. As a result, gold is used in a greater portion of the work [12].

There are two types of sensing mechanism in SPR technology. In case of internal sensing, the analyte selectively fills the air holes and in case of external sensing the analyte is placed outside the surface of the sensor. In recent years, several sensors using an internal sensing mechanism have been reported in the literature [9, 12, 13]. However, the internal sensing mechanism is not suitable for real-time and distributed sensing applications because of the need to change the analyte during measurement and also the emptying and refilling of selected air holes are difficult and time consuming. Moreover, internal sensing SPR sensors are difficult to fabricate and experience large propagation loss [14].

1.2 Photonic Crystal Fiber

Photonic-crystal fiber (PCF) is a class of optical fiber based on the properties of photonic crystals. It was first explored in 1996 at University of Bath, UK. Because of its ability to confine light in hollow cores or with confinement characteristics not possible in conventional optical fiber, PCF is now finding applications in fiber-optic communications, fiber lasers, nonlinear devices, high-power transmission, highly sensitive gas sensors, and other areas.

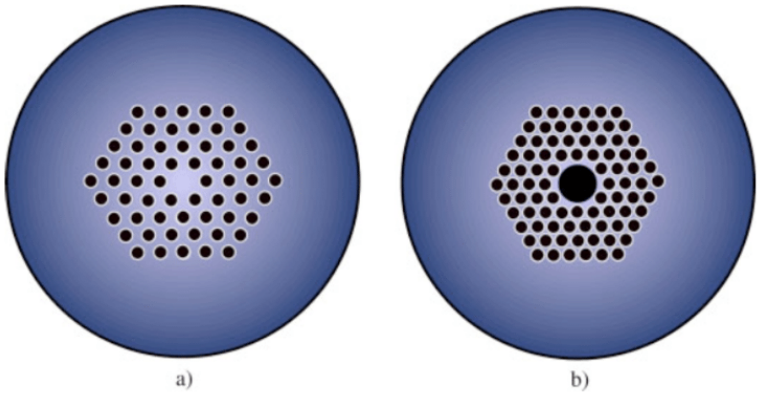

cl

Figure 1.1: Structure of photonic crystal fiber: a) index-guiding PCF, b) photonic bandgap PCF.

More specific categories of PCF include photonic-bandgap fiber (PCFs that confine light by

band gap effects), holey fiber (PCFs using air holes in their cross-sections), hole-assisted fiber (PCFs guiding light by a conventional higher-index core modified by the presence of air holes), and Bragg fiber (photonic-bandgap fiber formed by concentric rings of multilayer film). Photonic crystal fibers may be considered a subgroup of a more general class of microstructured optical fibers, where light is guided by structural modifications, and not only by refractive index differences.

Generally, such fibers are constructed by the same methods as other optical fibers: first, one constructs a ”preform” on the scale of centimeters in size, and then heats the preform and draws it down to a much smaller diameter (often nearly as small as a human hair), shrinking the preform cross section but (usually) maintaining the same features. In this way, kilometers of fiber can be produced from a single preform. The most common method involves stacking, although drilling/milling was used to produce the first aperiodic designs. This formed the subsequent basis for producing the first soft glass and polymer structured fibers.

1.3 Surface Plasmon Resonance

Surface plasmon resonance (SPR) is the resonant oscillation of conduction electrons at the interface between negative and positive permittivity material stimulated by incident light. SPR is the basis of many standard tools for measuring adsorption of material onto planar metal (typically gold or silver) surfaces or onto the surface of metal nanoparticles. It is the fundamental principle behind many color-based biosensor applications, different lab-on-a-chip sensors and diatom photosynthesis.

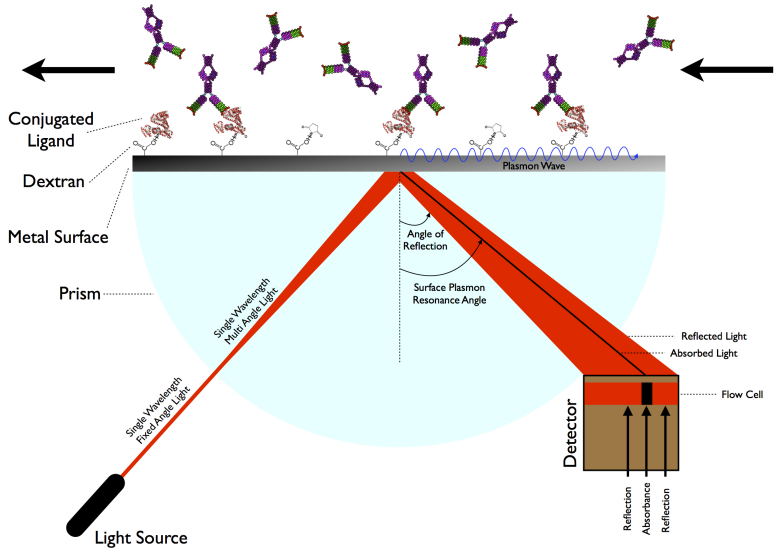

Figure 1.2: Surface plasmon resonance (SPR).

The surface plasmon polariton is a non-radiative electromagnetic surface wave that propagates

in a direction parallel to the negative permittivity/dielectric material interface. Since the wave is on the boundary of the conductor and the external medium (air, water or vacuum for example), these oscillations are very sensitive to any change of this boundary, such as the adsorption of molecules to the conducting surface.

To describe the existence and properties of surface plasmon polaritons, one can choose from various models (quantum theory, Drude model, etc.). The simplest way to approach the problem is to treat each material as a homogeneous continuum, described by a frequency-dependent relative permittivity between the external medium and the surface. This quantity, hereafter referred to as the materials' "dielectric function", is the complex permittivity. In order for the terms that describe the electronic surface plasmon to exist, the real part of the dielectric constant of the conductor must be negative and its magnitude must be greater than that of the dielectric. This condition is met in the infrared-visible wavelength region for air/metal and water/metal interfaces (where the real dielectric constant of a metal is negative and that of air or water is positive).

LSPRs (localized surface plasmon resonances) are collective electron charge oscillations in metallic nanoparticles that are excited by light. They exhibit enhanced near-field amplitude at the resonance wavelength. This field is highly localized at the nanoparticle and decays rapidly away from the nanoparticle/dieletric interface into the dielectric background, though far-field scattering by the particle is also enhanced by the resonance. Light intensity enhancement is a very important aspect of LSPRs and localization means the LSPR has very high spatial resolution (subwavelength), limited only by the size of nanoparticles. Because of the enhanced field amplitude, effects that depend on the amplitude such as magneto-optical effect are also enhanced by LSPRs.

1.4 Surface Plasmon Polariton

Surface plasmon polaritons (SPPs) are electromagnetic waves that travel along a metal–dielectric or metal–air interface, practically in the infrared or visible-frequency. The term "surface plasmon polariton" explains that the wave involves both charge motion in the metal ("surface plasmon") and electromagnetic waves in the air or dielectric ("polariton").

They are a type of surface wave, guided along the interface in much the same way that light can be guided by an optical fiber. SPPs are shorter in wavelength than the incident light (photons). Hence, SPPs can have tighter spatial confinement and higher local field intensity. Perpendicular to the interface, they have subwavelength-scale confinement. An SPP will propagate along the interface until its energy is lost either to absorption in the metal or scattering into other directions (such as into free space).

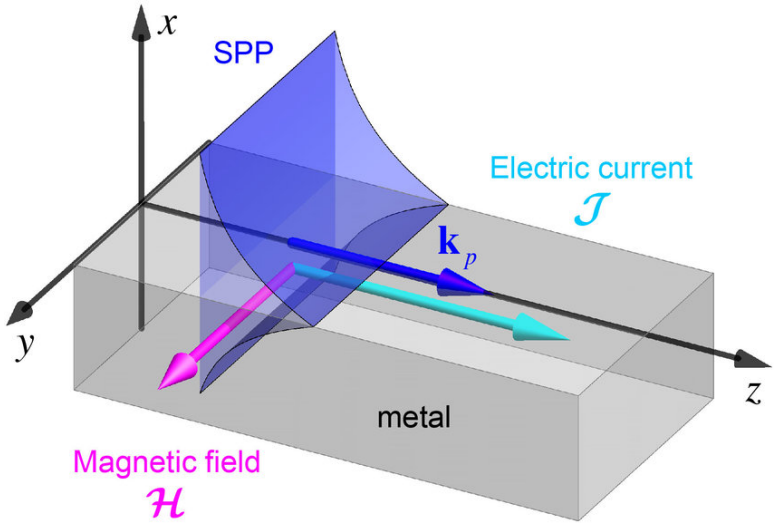

Figure 1.3: Surface plasmon polariton.

1.5 Optical Sensors

An optical sensor converts light rays into electronic signals. It measures the physical quantity of light and then translates it into a form that is readable by an instrument. An optical sensor is generally part of a larger system that integrates a source of light, a measuring device and the optical sensor. This is often connected to an electrical trigger. The trigger reacts to a change in the signal within the light sensor.

An optical sensor can measure the changes from one or several light beams. When a change occurs, the light sensor operates as a photoelectric trigger and therefore either increases or decreases the electrical output. An optical switch enables signals in optical fibres or integrated optical circuits to be switched selectively from one circuit to another.

1.6 Finite Element Method

The finite element method (FEM) is the most widely used method for solving problems of engineering and mathematical models. Typical problem areas of interest include the traditional fields of structural analysis, heat transfer, fluid flow, mass transport, and electromagnetic potential. The FEM is a particular numerical method for solving partial differential equations in two or three space variables (i.e., some boundary value problems).

To solve a problem, the FEM subdivides a large system into smaller, simpler parts that are called finite elements. This is achieved by a particular space discretization in the space dimensions, which is implemented by the construction of a mesh of the object: the numerical domain for the solution, which has a finite number of points.

The finite element method formulation of a boundary value problem finally results in a system of algebraic equations. The method approximates the unknown function over the domain. The simple equations that model these finite elements are then assembled into a larger system of equations that models the entire problem. The FEM then uses variational methods from the calculus of variations to approximate a solution by minimizing an associated error function.

1.7 Our Goal

Our goal is to study several recent and previous SPR sensors based on photonic crystal fiber and design a novel sensor with higher efficiency which can be fabricated with the existing technology.

Chapter 2

Brief Discussion: Optical Sensor

2.1 Working Principles

An optical sensor converts light rays into electronic signals. It measures the physical quantity of light and then translates it into a form that is readable by an instrument.

An optical sensor is generally part of a larger system that integrates a source of light, a measuring device and the optical sensor. This is often connected to an electrical trigger. The trigger reacts to a change in the signal within the light sensor. An optical sensor can measure the changes from one or several light beams. When a change occurs, the light sensor operates as a photoelectric trigger and therefore either increases or decreases the electrical output. An optical switch enables signals in optical fibres or integrated optical circuits to be switched selectively from one circuit to another.

An optical switch can operate by mechanical means or by electro-optic effects, magneto-optic effects as well as by other methods. Optical switches are optoelectronic devices which can be integrated with integrated or discrete microelectronic circuits.

2.2 Cross-section

Air Hole

PCF air holes are arranged on the vertex of an equilateral triangle with six air holes in the first ring around the core, which is called the HPCF. Beside the hexagonal structure other structures such as, square lattice, cob web, honeycomb, octagonal and decagonal are proposed for the design of PCF.

Pitch Distance

”Pitch” is widely used to describe the distance between repeated elements in a structure possessing translational symmetry. PCD is the short form of Pitch Circle Diameter; the Pitch Circle Diameter (PCD) is the diameter of that circle which passes through the center of all the bolts hole or wheel bolts or wheel rim holes or stud. The best example is Flanges, there are multiple holes in Flanges, the circle through the center of these holes is known as pitch circle and the diameter of this circle is known as Pitch Circle Diameter, in short PCD.

Background Material

Generally, we use different glasses and plastics as background material. In our experiment, we have decided to use fused silica as background material.

Metallic Layer

In plasmonics, we study the effect of electromagnetic wave in metal i.e. gold, silver etc. Light, when propagates through the waveguide, two of its vector components create two phenomena. The component along with the waveguide, is responsible for light propagation. On the other hand, the component, perpendicular to the propagation line, is responsible for an interesting phenomena, called surface plasmon polariton. Photons of incoming light excite the surface electrons of plasmonic layer. We can use this information, for our experiment.

Analyte Layer

Our thesis is based on biosensors and sensing applications. So, in our device, there must be a place included for analyte to be detected. We can include the place holder inside or outside the fiber depending on the sensing method.

There are two sensing method, internal and external. In external sensing, the analyte place holder is adjacent to the outer wall of the plasmonic layer. The EM wave excites the surface electrons of plasmonic layer, this excitation transmits to the analyte molecules. Hence, we get the ultimate information to detect the analyte.

In internal sensing, an appropriate air hole is selected to be the analyte place holder. This is good in detection, but difficult in implication. Throughout our thesis, we use the external sensing method.

Perfectly Matched Layer

A perfectly matched layer (PML) is an artificial absorbing layer for wave equations, commonly used to truncate computational regions in numerical methods to simulate problems with open boundaries, especially in the FDTD and FE methods. The key property of a PML that distinguishes it from an ordinary absorbing material is that it is designed so that waves incident upon the PML from a non-PML medium do not reflect at the interface—this property allows the PML to strongly absorb outgoing waves from the interior of a computational region without reflecting them back into the interior.

PML was originally formulated by Berenger in 1994 for use with Maxwell's equations, and since that time there have been several related reformulations of PML for both Maxwell's equations and for other wave-type equations, such as elastodynamics, the linearized Euler equations, Helmholtz equations, and poroelasticity.

Berenger's original formulation is called a split-field PML, because it splits the electromagnetic fields into two unphysical fields in the PML region. A later formulation that has become more popular because of its simplicity and efficiency is called uniaxial PML or UPML, in which the PML is described as an artificial anisotropic absorbing material. Although both Berenger's formulation and UPML were initially derived by manually constructing the conditions under which incident plane waves do not reflect from the PML interface from a homogeneous medium, both formulations were later shown to be equivalent to a much more elegant and general approach: stretched-coordinate PML.

In particular, PMLs were shown to correspond to a coordinate transformation in which one (or more) coordinates are mapped to complex numbers; more technically, this is actually an analytic continuation of the wave equation into complex coordinates, replacing propagating (oscillating) waves by exponentially decaying waves. This viewpoint allows PMLs to be derived for inhomogeneous media such as waveguides, as well as for other coordinate systems and wave equations.

PML is widely used and has become the absorbing boundary technique of choice in much of computational electromagnetism. Although it works well in most cases, there are a few important cases in which it breaks down, suffering from unavoidable reflections or even exponential growth.

One caveat with perfectly matched layers is that they are only reflectionless for the exact, continuous wave equation. Once the wave equation is discretized for simulation on a computer, some small numerical reflections appear (which vanish with increasing resolution).

For this reason, the PML absorption coefficient is typically turned on gradually from zero (e.g. quadratically) over a short distance on the scale of the wavelength of the wave. In general, any absorber, whether PML or not, is reflectionless in the limit where it turns on sufficiently

gradually (and the absorbing layer becomes thicker), but in a discretized system the benefit of PML is to reduce the finite-thickness ”transition” reflection by many orders of magnitude compared to a simple isotropic absorption coefficient.

2.3 Performance Matrices

Confinement Loss

Confinement losses are the losses arising from the leaky nature of the modes and the non-perfect structure of the PCF fiber. Then, depending on the wavelength, number of holes rings, and hole size, modes will be guided with a structure dependent loss.

Confinement loss of the proposed sensor can be calculated by using the imaginary part of the complex RI by using the following equation [15],

$$\alpha_{loss} = 8.856 \times \frac{2\pi}{\lambda} \times Im(n_{eff}) \times 10^4 dB/cm. \tag{2.1}$$

Wavelength and Amplitude Interrogation

We evaluate the performance of the proposed sensor using both amplitude interrogation (AI) and wavelength interrogation (I) method. According to WI method the wavelength sensitivity can be calculated according to the following equation [16],

$$S_W(\lambda) = \frac{\Delta\lambda_{peak}}{\Delta n_a} \tag{2.2}$$

where, $\Delta\lambda_{\text{peak}}$ and Δn_a denotes the shift in resonance peaks and analyte RI respectively.

The amplitude sensitivity of the sensor can be calculated according to the following equation [17],

$$S_A(\lambda) = -\frac{1}{\alpha(\lambda, n_a)} \frac{\delta\alpha(\lambda, n_a)}{\delta n_a} \tag{2.3}$$

where, the difference between two loss spectra due to any tiny-tiny little change of analyte RI is denoted by $\delta\alpha$, λ, n_a and δn_a indicates the change in analyte RI.

Sensor Resolution

Sensor resolution is a very important parameter which determines the degree of detection with variation of analyte RI. This can be calculated by the following equation [18],

$$R = \frac{\Delta n_a \Delta \lambda_{min}}{\Delta \lambda_{peak}}. \tag{2.4}$$

Here, R, Δn_a, $\Delta \lambda_{min}$, $\Delta \lambda_{peak}$ represents the sensor resolution, the variation of analyte RI, the minimum wavelength resolution, and the difference in resonance peak shift respectively.

Birefringence

Birefringence determines the polarization states of a fiber that is defined as the RI difference between the polarization modes. This can be calculated by the following equation [18],

$$B = \mid n_x - n_y \mid \tag{2.5}$$

Chapter 3

Our Design

Throughout the chapter, we will briefly discuss two of our designed SPR biosensor based on photonic crystal fiber. Later on, we will compare the sensors.

3.1 Objective

Lots of designs are already published in many well known literature. Researchers are continuously upgrading their design with better performance. But, too few designs satisfies all the performance matrices. There is a trade-off among them. After a through study, our team has decided to design a sensor with a dynamic sensing range, so that, one can detect a wide range of bio-molecules with only a single sensing device.

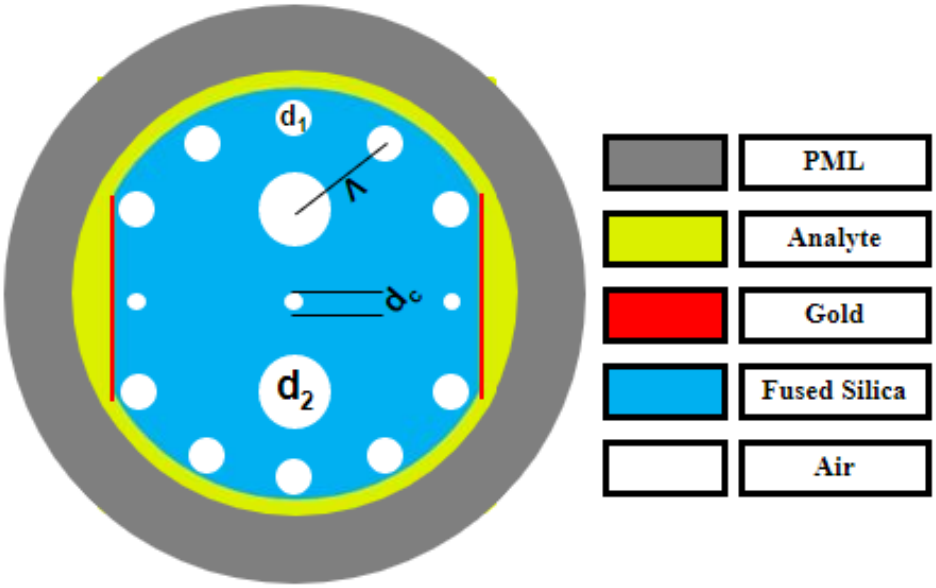

Figure 3.1: Cross section of Design 1.

3.2 Design 1: Dual Side Polished

Throughout the study, we have found different type of sensor cross section. Like everything else, they have their pros and cons. Each design has unique features. Recently, sensors with polished wall have been mentioned in many well known international Journals and conference paper. In many literature this type of shape had been introduced as D-shaped sensor. Fabrication of the polished structure is bit complex than the conventional one. But, sensitivity of the polished structure is generally better. Moreover, reuse of the polished structure is easy and, this is remarkable.

In recent time, several literature mentioned dual side polished structure. We realize an important phenomenon; in single side polished structure, light touches one wall of plasmonic material. If we increase the channel, through which light can touch the plasmonic material, we can achieve better sensitivity. In polished shape, light has to travel shorter path to touch the plasmonic wall than the conventional pcf. Furthermore, in dual polished structure we get addition advantage; light has a shorter path to travel and increased channel to propagate. This is amazing.

3.2.1 Numerical Analysis

We design and numerical analyse the sensor with COMSOL Multiphysics version 5.3 and 5.5. Data set is collected after simulation of the model in COMSOL. Using the data set, several figures are plotted in MATLAB.

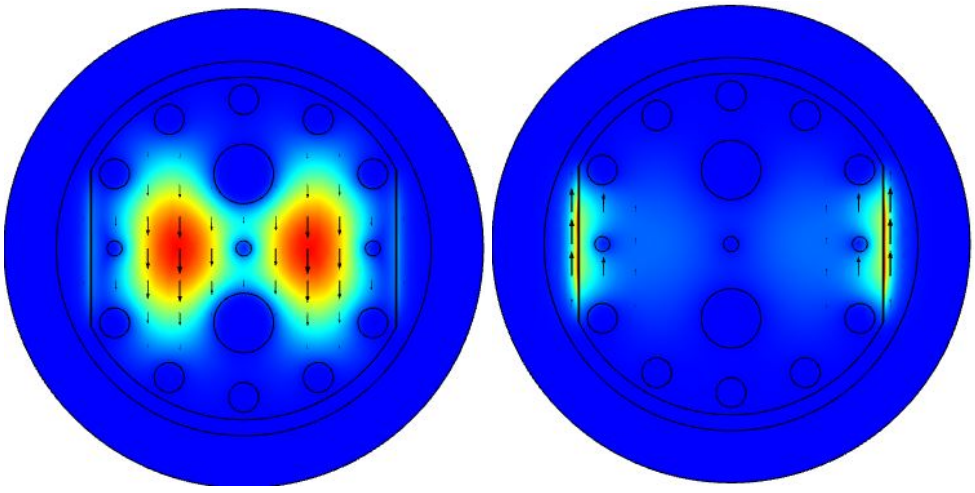

(a) (b)

Figure 3.2: Electrical field distribution in a core and b spp mode.

We have used finite element method (FEM) based software COMSOL version 5.5 to model and evaluate the performance of the proposed sensor. The schematic of the proposed sensor has been shown in Fig. **??**.

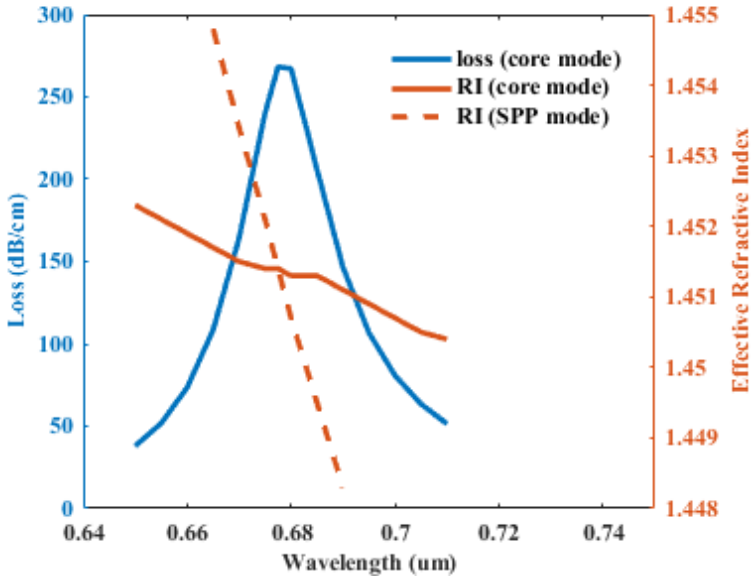

Figure 3.3: Phase-matching of core and SPP mode for optimized parameters.

Physics-controlled mesh sequence with normal element size has been used in simulation. We have shown the electric field distribution of core mode and SPP mode in Fig. 3.2a, 3.2b respectively. The phase-matching of core and SPP mode is presented in Fig. 3.3.

A circular air hole based circular shaped cladding is proposed in a silica (SiO_2) substrate. Different diameters of air holes (d_c, d_1, d_2, d_3) have been used to shape the cladding. We optimize the air hole diameters (d_c, d_1, d_2 and d_3), pitch distance (Λ), gold (t_g), analyte (t_a) and PML (t_p) thickness to determine the optimal design conditions. After careful investigation we choose Λ = 2 µm, d_1 = 0.8 µm, d_2 = 1.6 µm, d_3 = d_c = 400 nm, t_g = 40nm, t_a = 0.35 µm, and t_p = 1.4 µm as optimal.

With this optimal values, we have presented amplitude sensitivity and confinement loss curve in Fig. 3.4 and Fig. 3.5 respectively for a wide range of analytes.

The material dispersion of pure silica can be calculated using the Sellmier equation, which is valid for the wavelength region of 0.37 to 2.2 µm [19]. The material dispersion of gold can be determined from the Drude-Lorentz model [20, 21].

Confinement loss of the proposed sensor can be calculated by using the imaginary part of the complex RI by using the equation (2.1), [15].

Note that the performance evaluation of the proposed sensor is carried out using both wavelength interrogation (WI) and amplitude interrogation (AI) method. According to WI method the wavelength sensitivity can be calculated according to the following equation (2.2), [16].

The amplitude sensitivity of the sensor can be calculated according to the equation (2.3), [17].

Sensor resolution is also an important parameter that determines the degree of detection with

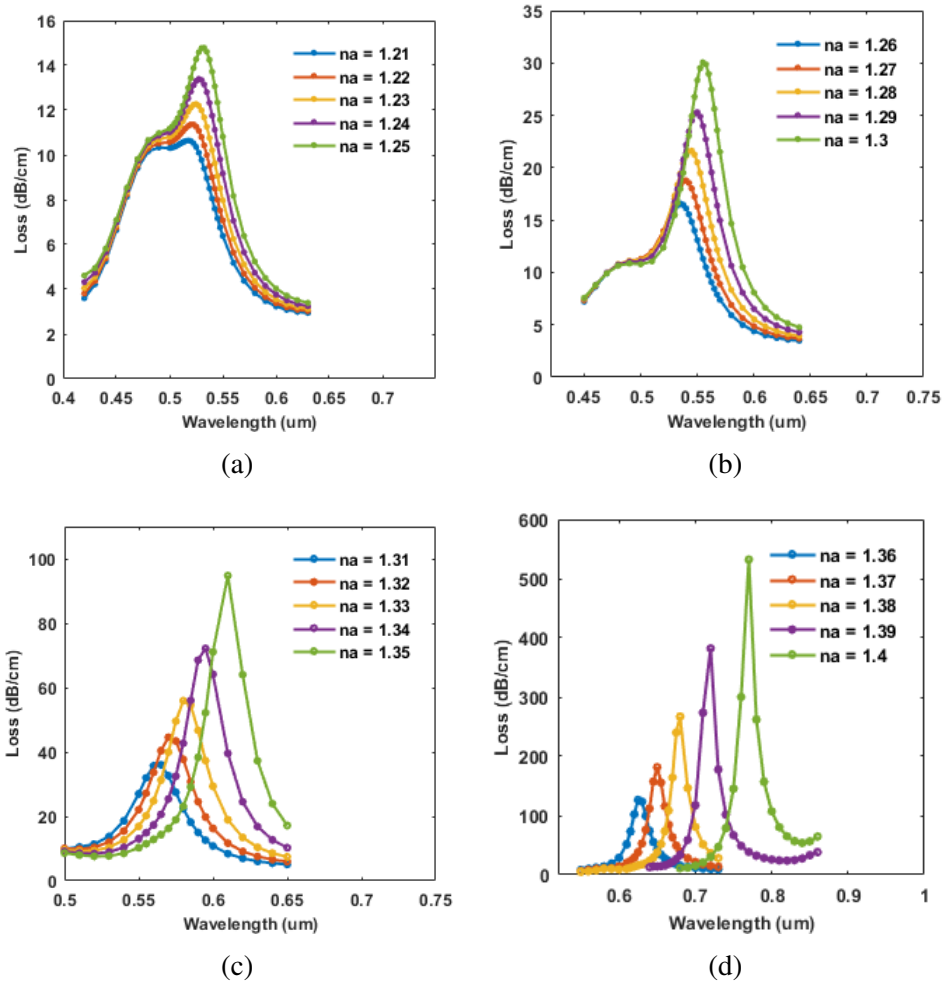

Figure 3.4: Confinement loss for a na = 1.21-1.25, b na = 1.26-1.3, c na = 1.31-1.35 and d na = 1.36-1.34.

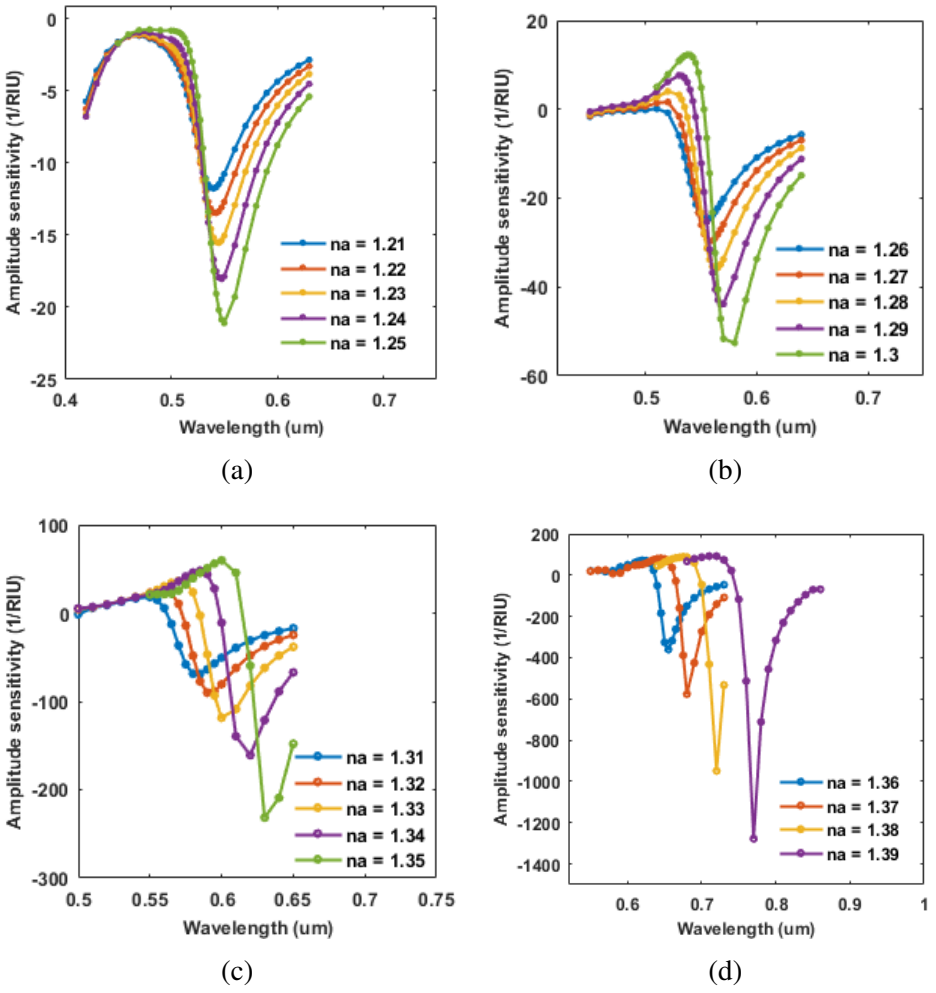

Figure 3.5: Amplitude sensitivity for a na = 1.21-1.25, b na = 1.26-1.3, c na = 1.31-1.35 and d na = 1.36-1.39.

analyte RI variation. The resolution of a sensor can be determined by the equation (2.4), [18].

3.2.2 Parameters Optimization

We have observed the sensor performance shown in Fig. **??** by varying different parameters for choosing the optimum value.

We have found that for a particular RI, increasing the value of d_1 results in a positive vertical shift of the loss curve and the resonance wavelength remains almost unchanged. We choose d_1 = 2 µm as optimal value as there is a sharp peak at the resonance wavelength.

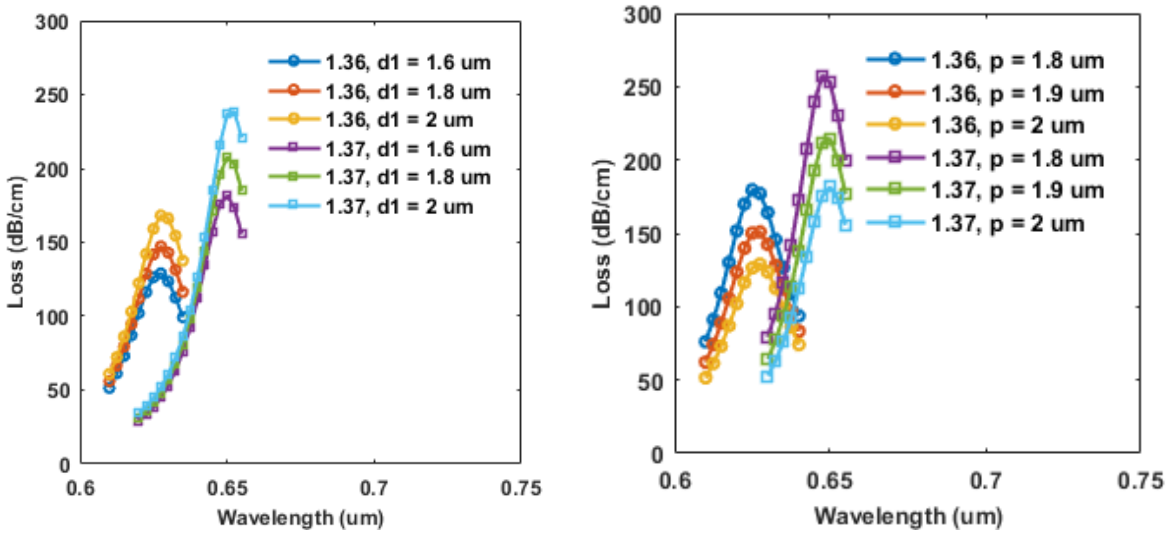

(a) (b)

Figure 3.6: Effect of a air hole diameter (d_1) and b pitch distance (Λ).

There is a negative vertical shift with the increase of pitch Λ. The resonance wavelength is almost independent of the pitch distance. We choose the pitch distance, Λ = 2 µm, as the confinement loss is low here.

We found an almost independent nature of the sensor with respect to the analyte and PML thickness.

Thickness of gold has a significant effect on both the amplitude and the wavelength sensitivity. Therefore, it influences the overall performance of the sensor. As shown in the fig. there is a positive horizontal shift and a negative vertical shift with the increase of gold thickness. For a particular analyte, a thicker gold layer results in a broader loss peak and an increased SNR of the sensor. So, we've selected the optimum thickness for the gold layer to be 40 nm.

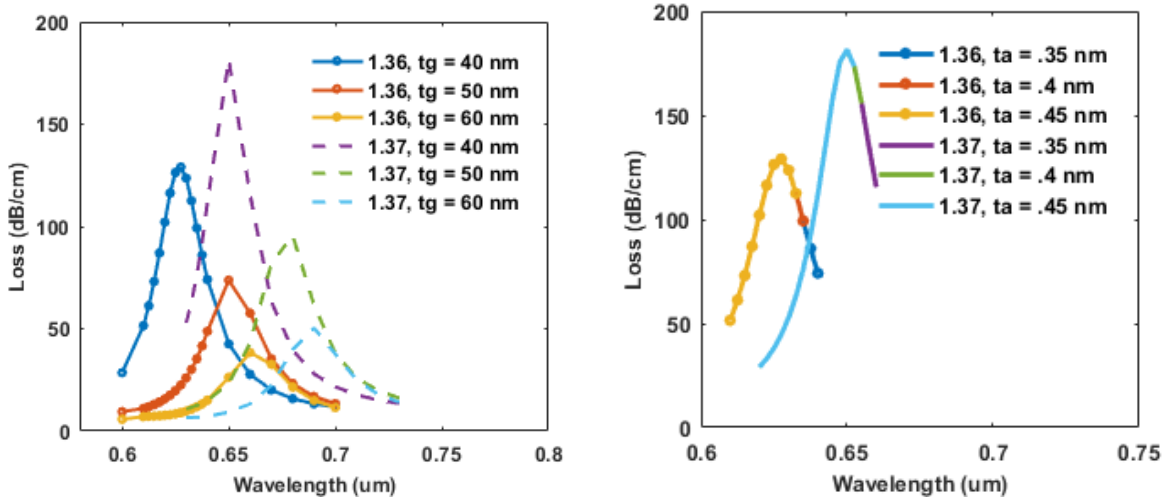

(a) (b)

Figure 3.7: Effect of a gold layer thickness (t_g) and b analyte thickness (t_a).

3.3 Design 2: Circular

After analysing the dual side polished sensor our supervisor told us to repeat the process without polishing the fiber. So, according to his guidance, we have changed the geometry of the

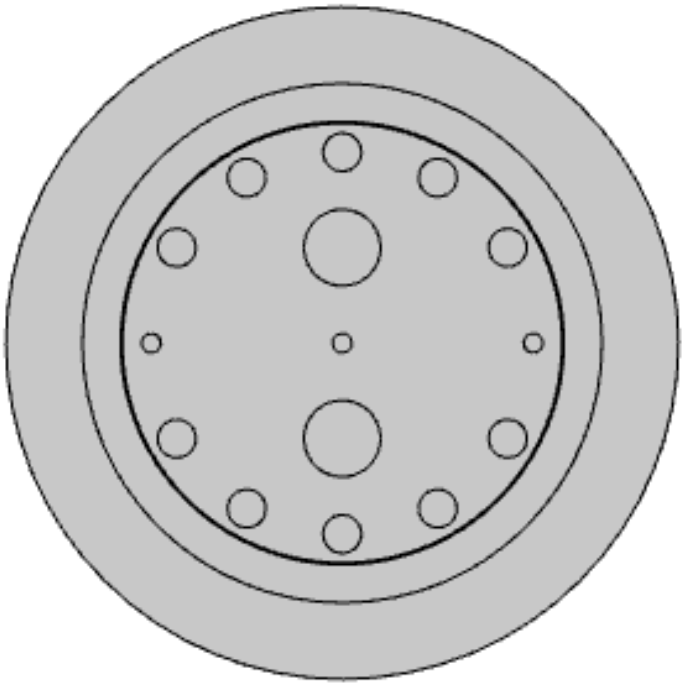

Figure 3.8: Cross section of Design 2.

structure. The model is given in fig. 3.8.

With the optimized parameter, same as design 1, we obtain the confinement loss and amplitude sensitivity curves. Confinement loss curves are shown in fig. 3.9 and amplitude sensitivity curves are presented in fig. 3.10.

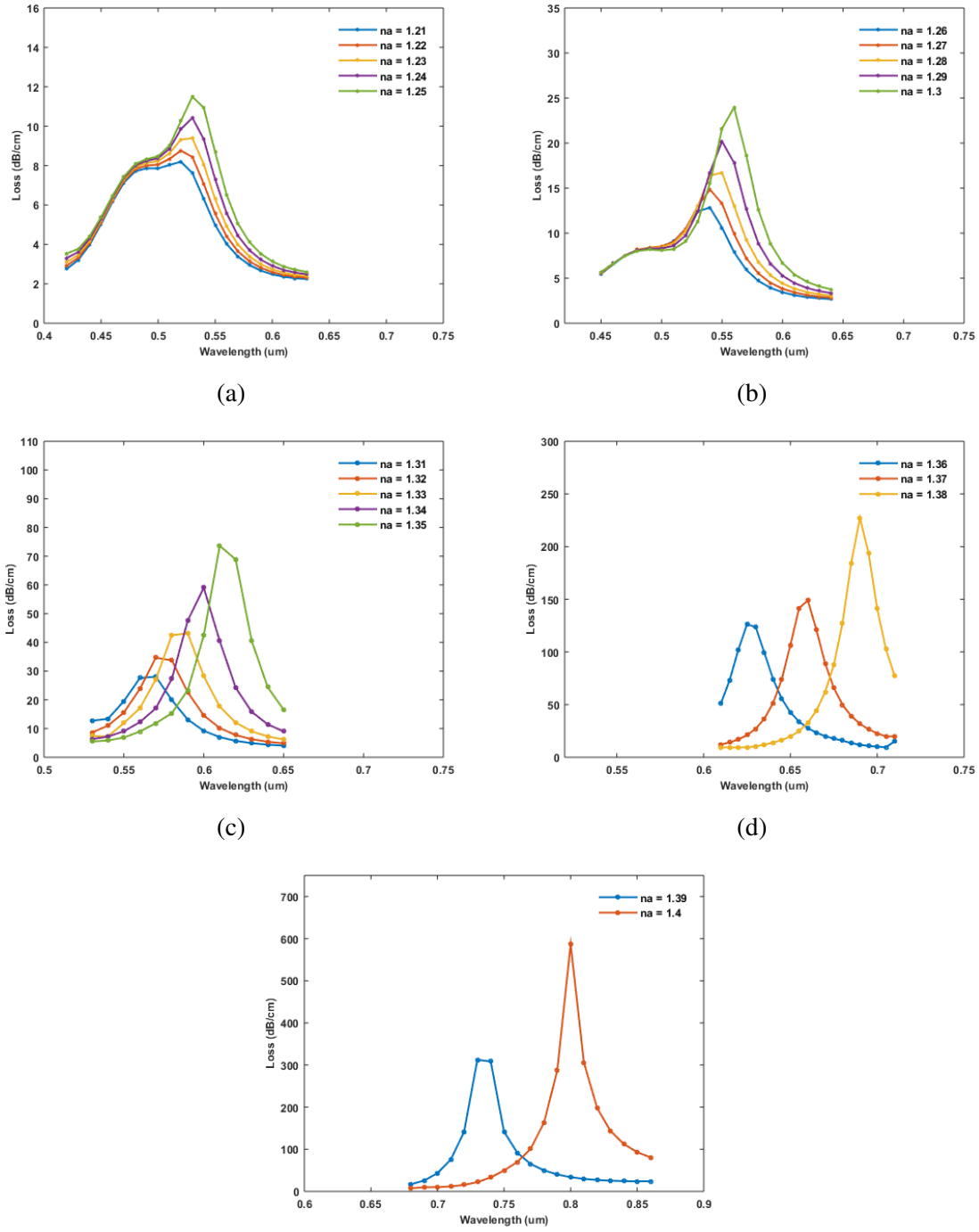

Figure 3.9: Confinement loss fora) na = 1.21-1.25, b na = 1.26-1.3, c na = 1.31-1.35, d na = 1.36-1.38 and e na = 1.39-1.4.

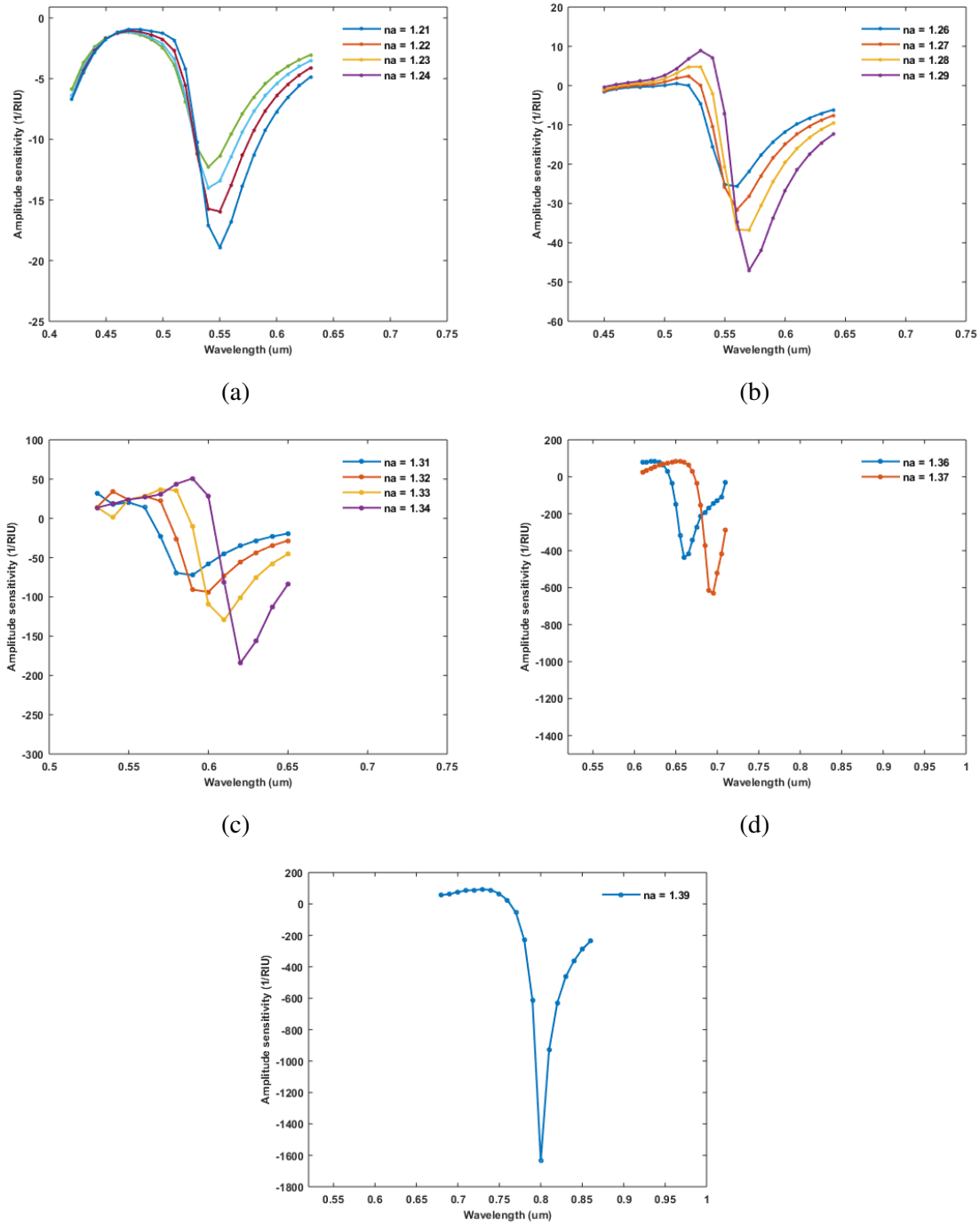

Figure 3.10: Amplitude sensitivity for a na = 1.21-1.24, b na = 1.26-1.29, c na = 1.31-1.34, d and e na =1.39.

3.3.1 Numerical Analysis

We analyse design 2 like the previous one. We use the same software and equations for calculation. The sensing range is same as before. We have found the maximum AS of 1600/RIU and maximum WS of 7000 nm/RIU.

3.4 Comparison With Previously Reported Sensors

Ref.	Sensing Approach	RI Range	Max. W. S. (nm/RIU)	Max. Amp. Sens.(1/RIU)	Sensor Resolution
[6]	External(Dual Side Polished)	1.23-1.29	5500	333.8	7.69×10^{-6}
[8]	External(Side Polished)	1.33-1.35	17000	74	5.8×10^{-5}
[10]	External	1.33-1.37	5000	860	4×10^{-5}
[12]	External(Multi Channel)	1.32-1.36	4600	425	2×10^{-5}
[21]	Internal(Multi Coated)	1.45-1.49	-5500	-	-
[24]	Internal(Selectively Coated)	1.33-1.42	11000	1420	9.1×10^{-5}
[44]	Internal(Multi Coated)	1.34-1.48	1131	-	1×10^{-4}
[45]	External(Side Polished)	1.346-1.410	12450	-	8.03×10^{-6}
[46]	External(Side Polished)	1.28-1.34	6000	178	0.16×10^{-6}
[26]	External(Side Polished)	1.33-1.43	46000	1086	2.2×10^{-5}
[31]	External(Dual side polished)	1.36-1.41	14660	1222	6.82×10^{-6}
[47]	External(Multi core flat fiber)	1.46-1.485	23000	820	4.35×10^{-6}
[48]	External	1.33-1.38	4600	420.4	2.17×10^{-5}
[49]	External	1.40-1.43	15180	498	5.68×10^{-6}
[50]	External	1.33-1.43	62000	1415	1.61×10^{-6}
[51]	External(Exposed core localized)	1.32-1.41	34000	1170	2.94×10^{-6}
[52]	External(Side polished)	1.18-1.36	20000	1054	5×10^{-6}
[53]	External	1.32-1.40	23000	-	4.34×10^{-6}
[54]	External(Side polished)	1.00-1.37	20000	811	5×10^{-6}
[55]	External(Dual side polished)	1.395-1.415	12400	252	9.39×10^{-6}
[56]	External(Side polished)	1.29-1.39	116000	2452	8.62×10^{-7}
Design 1	External(Dual side polished)	1.21-1.4	5000	1277.47	2×10^{-5}
Design 2	External	1.21-1.4	7000	1600	1.4×10^{-5}

Chapter 4

Conclusion

A circular and a dual side polished PCF based SPR sensor have been designed. Dual side polished structure has a maximum wavelength sensitivity of 5000 nm/RIU and maximum amplitude sensitivity of 1277.47 RIU^{-1} within the analyte RI of 1.21 to 1.40. The sensor also shows a maximum resolution of 2×10^{-5}.

Circular structure has a maximum wavelength sensitivity of 7000 nm/RIU and maximum amplitude sensitivity of 1600 RIU^{-1} within the analyte RI of 1.21 to 1.40. The sensor also shows a maximum resolution of 1.4×10^{-5}.

To our knowledge our obtained sensing range is wider than almost any prior reported PCF-SPR sensors. We can detect a wide range of biomolecules with only a single sensor. Moreover, The fabrication of the sensor is straightforward with existing technologies.

References

[1] E. Kretschmann and H. Raether, "Radiative decay of non-radiative surface plasmons excited by light," *Z. Naturforsch. a*, vol. 23, no. 12, pp. 2135–2136, 1968.

[2] L. G. Carrascosa, A. A. I. Sina, R. Palanisamy, B. Sepulveda, M. A. Otte, S. Rauf, M. J. Shiddiky, and M. Trau, "Molecular inversion probe-based spr biosensing for specific, label-free and real-time detection of regional dna methylation," *Chemical communications*, vol. 50, no. 27, pp. 3585–3588, 2014.

[3] B. Lee, S. Roh, and J. Park, "Current status of micro-and nano-structured optical fiber sensors," *Optical Fiber Technology*, vol. 15, no. 3, pp. 209–221, 2009.

[4] C. Liu, L. Yang, X. Lu, Q. Liu, F. Wang, J. Lv, T. Sun, H. Mu, and P. K. Chu, "Mid-infrared surface plasmon resonance sensor based on photonic crystal fibers," *Optics Express*, vol. 25, no. 13, pp. 14227–14237, 2017.

[5] G. Robinson, "The commercial development of planar optical biosensors," *Sensors and Actuators B: Chemical*, vol. 29, no. 1-3, pp. 31–36, 1995.

[6] J. N. Dash and R. Jha, "Highly sensitive side-polished birefringent pcf-based spr sensor in near ir," *Plasmonics*, vol. 11, no. 6, pp. 1505–1509, 2016.

[7] J. N. Dash and R. Jha, "Graphene-based birefringent photonic crystal fiber sensor using surface plasmon resonance," *IEEE Photonics Technology Letters*, vol. 26, no. 11, pp. 1092–1095, 2014.

[8] R. Otupiri, E. K. Akowuah, and S. Haxha, "Multi-channel spr biosensor based on pcf for multi-analyte sensing applications," *Optics express*, vol. 23, no. 12, pp. 15716–15727, 2015.

[9] J. Xue, S. Li, Y. Xiao, W. Qin, X. Xin, and X. Zhu, "Polarization filter characters of the gold-coated and the liquid filled photonic crystal fiber based on surface plasmon resonance," *Optics express*, vol. 21, no. 11, pp. 13733–13740, 2013.

[10] Y. Lu, X. Yang, M. Wang, and J. Yao, "Surface plasmon resonance sensor based on hollow-core pcfs filled with silver nanowires," *Electronics Letters*, vol. 51, no. 21, pp. 1675–1677, 2015.

[11] A. A. Rifat, G. A. Mahdiraji, D. M. Chow, Y. G. Shee, R. Ahmed, and F. R. M. Adikan, "Photonic crystal fiber-based surface plasmon resonance sensor with selective analyte channels and graphene-silver deposited core," *Sensors*, vol. 15, no. 5, pp. 11499–11510, 2015.

[12] R. Zakaria, W. Kam, Y. Ong, S. Yusoff, H. Ahmad, and W. S. Mohammed, "Fabrication and simulation studies on d-shaped optical fiber sensor via surface plasmon resonance," *Journal of Modern Optics*, vol. 64, no. 14, pp. 1443–1449, 2017.

[13] L. Duan, X. Yang, Y. Lu, and J. Yao, "Hollow-fiber-based surface plasmon resonance sensor with large refractive index detection range and high linearity," *Applied Optics*, vol. 56, no. 36, pp. 9907–9912, 2017.

[14] A. A. Rifat, R. Ahmed, G. A. Mahdiraji, and F. M. Adikan, "Highly sensitive d-shaped photonic crystal fiber-based plasmonic biosensor in visible to near-ir," *IEEE Sensors Journal*, vol. 17, no. 9, pp. 2776–2783, 2017.

[15] A. Hassani and M. Skorobogatiy, "Design criteria for microstructured-optical-fiber-based surface-plasmon-resonance sensors," *JOSA B*, vol. 24, no. 6, pp. 1423–1429, 2007.

[16] C. Liu, W. Su, Q. Liu, X. Lu, F. Wang, T. Sun, and P. K. Chu, "Symmetrical dual d-shape photonic crystal fibers for surface plasmon resonance sensing," *Optics express*, vol. 26, no. 7, pp. 9039–9049, 2018.

[17] B. Gauvreau, A. Hassani, M. F. Fehri, A. Kabashin, and M. Skorobogatiy, "Photonic bandgap fiber-based surface plasmon resonance sensors," *Optics express*, vol. 15, no. 18, pp. 11413–11426, 2007.

[18] M. Hautakorpi, M. Mattinen, and H. Ludvigsen, "Surface-plasmon-resonance sensor based on three-hole microstructured optical fiber," *Optics express*, vol. 16, no. 12, pp. 8427–8432, 2008.

[19] I. H. Malitson, "Interspecimen comparison of the refractive index of fused silica," *Josa*, vol. 55, no. 10, pp. 1205–1209, 1965.

[20] P. J. Sazio, A. Amezcua-Correa, C. E. Finlayson, J. R. Hayes, T. J. Scheidemantel, N. F. Baril, B. R. Jackson, D.-J. Won, F. Zhang, E. R. Margine, *et al.*, "Microstructured optical fibers as high-pressure microfluidic reactors," *Science*, vol. 311, no. 5767, pp. 1583–1586, 2006.

[21] A. Vial, A.-S. Grimault, D. Macías, D. Barchiesi, and M. L. De La Chapelle, "Improved analytical fit of gold dispersion: Application to the modeling of extinction spectra with a finite-difference time-domain method," *Physical Review B*, vol. 71, no. 8, p. 085416, 2005.

Appendix A

MATLAB Codes

A.1 Code Snippet For Plotting Amplitude Sensitivity

```
clc;
close all;
clear all;
%%
file = 'H:\SPR\My_Design\TSP model\tg=40nm\A.S..xlsx';
l = xlsread(file, 3, 'A:A');
as_a1 = xlsread(file, 3, 'O:O');
as_a2 = xlsread(file, 3, 'P:P');
as_a3 = xlsread(file, 3, 'Q:Q');
as_a4 = xlsread(file, 3, 'R:R');
as_a5 = xlsread(file, 3, 'S:S');
%%
plot(l, as_a1, '-o', 'LineWidth', 1.5, 'MarkerSize', 2);
hold on

plot(l, as_a2, '-o', 'LineWidth', 1.5, 'MarkerSize', 2);
hold on

plot(l, as_a3, '-o', 'LineWidth', 1.5, 'MarkerSize', 2);
hold on

plot(l, as_a4, '-o', 'LineWidth', 1.5, 'MarkerSize', 2);
hold on

```

```
plot(l(4:end), as_a5, '-o', 'LineWidth', 1.5, 'MarkerSize', 2);

xlabel('Wavelength (um)');
ylabel('Amplitude sensitivity (1/RIU)');

hold off

legend('na = 1.21', 'na = 1.22', 'na = 1.23', 'na = 1.24', 'na = 1.25');
legend('boxoff')

set(findall(gcf, '-property', 'FontSize'), 'FontSize', 9)
set(findall(gcf, '-property', 'FontWeight'), 'FontWeight', 'bold')

axis([.4 .75 -25 .9])
```

A.2 Code Snippet For Plotting Confinement Loss

```
clc;
close all;
clear all;
%%
file = 'H:\SPR\My_Design\TSP model\tg=40nm\A.S..xlsx';
l = xlsread(file, 3, 'A:A');
loss_a1 = xlsread(file, 3, 'C:C');
loss_a2 = xlsread(file, 3, 'E:E');
loss_a3 = xlsread(file, 3, 'G:G');
loss_a4 = xlsread(file, 3, 'I:I');
loss_a5 = xlsread(file, 3, 'K:K');
%%
plot(l, loss_a1, '-o', 'LineWidth', 1.5, 'MarkerSize', 2);
hold on

plot(l, loss_a2, '-o', 'LineWidth', 1.5, 'MarkerSize', 2);
hold on

plot(l, loss_a3, '-o', 'LineWidth', 1.5, 'MarkerSize', 2);
hold on

plot(l, loss_a4, '-o', 'LineWidth', 1.5, 'MarkerSize', 2);
```

```
23 hold on
24
25 plot(l, loss_a5, '-o', 'LineWidth', 1.5, 'MarkerSize', 2);
26
27 xlabel('Wavelength (um)');
28 ylabel('Loss (dB/cm)');
29
30 hold off
31
32 legend('na = 1.21', 'na = 1.22', 'na = 1.23', 'na = 1.24', 'na = 1.25');
33 legend('boxoff')
34
35 set(findall(gcf, '-property', 'FontSize'), 'FontSize', 9)
36 set(findall(gcf, '-property', 'FontWeight'), 'FontWeight', 'bold')
37
38 axis([.4 .75 0 16])
```

Generated using Undegraduate Thesis LaTeX Template, Version 1.4. Department of Electrical and Electronic Engineering, Bangladesh University of Engineering and Technology, Dhaka, Bangladesh.

This thesis was generated on Tuesday 9th February, 2021 at 6:00pm.